First-time analysis of detached divertor conditions in RMP ELM suppressed H-mode plasma in ITER

H. Frerichs[1], X. Bonnin[2], Y. Feng[3], L. Li[4], Y. Q. Liu[5], A. Loarte[2], R. A. Pitts[2], D. Reiter[6], O. Schmitz[1]

[1] University of Wisconsin - Madison, Department of Engineering Physics, Madison, WI, USA
[2] ITER Organization, Route de Vinon-sur-Verdon, CS 90 046, 13067 St Paul Lez Durance Cedex, France
[3] Max-Planck-Institut für Plasmaphysik, Association EURATOM-IPP, 17491 Greifswald, Germany
[4] College of Science, Donghua University, Shanghai 201620, China
[5] General Atomics, PO Box 85608, San Diego, CA 92186-5608, USA
[6] Institute for Laser and Plasma Physics, Heinrich-Heine-University, D-40225 Duesseldorf, Germany

Third IAEA Technical Meeting on Divertor Concepts, 4-7 November, 2019, Vienna, Austria

Acknowledgements: This work was supported by the U.S. Department of Energy under grants DE-SC0012315, DE-SC0013911 and DE-SC0020357, by the College of Engineering at the University of Wisconsin - Madison, and by the ITER Scientist Fellow Network. The views and opinions expressed herein do not necessarily reflect those of the ITER Organization.

3dpsi.engr.wisc.edu

iter
china eu india japan korea russia usa

College of Engineering
UNIVERSITY OF WISCONSIN–MADISON

Motivation: compatibility of detached divertor plasmas with RMPs for ELM control

- Control of divertor loads is required for next step magnetic fusion devices $\rightarrow$ **detached plasma operation**
- **Resonant magnetic perturbations (RMPs)** will be used for ELM control in ITER
- A **3D plasma edge model** (EMC3-EIRENE) is required to analyze the impact on divertor performance

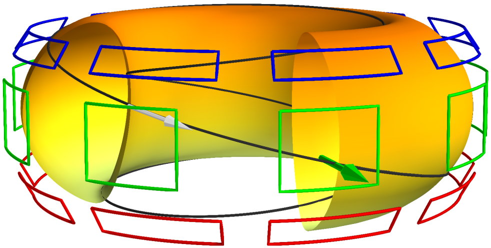

- Staged Approach: Pre-Fusion Power Operation (PFPO): $P_{\mathrm{SOL}} = 30\,\mathrm{MW}$, $B_t/I_p = 1.8\,\mathrm{T}/5\,\mathrm{MA}$, $q_{95} = 3$
- Focus on $n = 3$ RMP field with coil phasing optimized for ELM control

Outline

EMC3-EIRENE extends the traditional (axisymmetric) framework for divertor perfomance analysis to 3 dimensions

- Magnetic geometry is input for plasma boundary modeling

Geometry

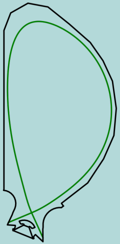

Magnetic field (equilibrium)

Divertor design

Model parameters

2D Plasma boundary model

SOLPS-4.3 / SOLPS-ITER

Plasma ⟳ Neutral gas

Simulation data

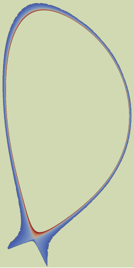

Density

Temperature

Divertor loads

- Boundary plasma is determined by particle, momentum, and energy balances

EMC3-EIRENE extends the traditional (axisymmetric) framework for divertor perfomance analysis to 3 dimensions

- Magnetic geometry is input for plasma boundary modeling and can include **plasma response** effects (MARS-F, . . .)

Geometry

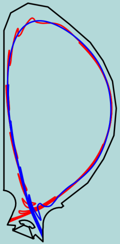

Magnetic field (equilibrium + RMPs)

Divertor design

Model parameters

3D Plasma boundary model

EMC3-EIRENE

Plasma ⟳ Neutral gas

Simulation data

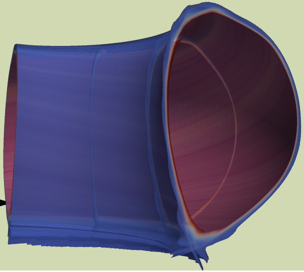

- Boundary plasma is determined by particle, momentum, and energy balances

Outline

Resistive single fluid calculations (MARS-F) show strong screening of resonant field components

- Ideal magneto-hydrodynamics (MHD) suggests screening of resonant fields

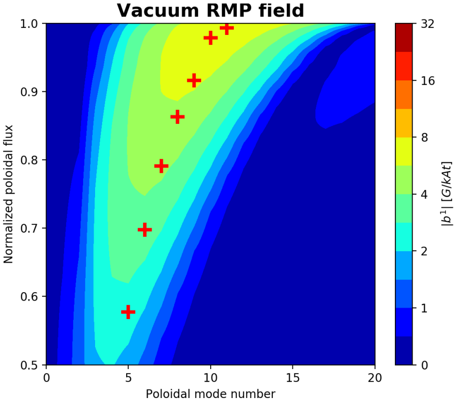

Resistive single fluid calculations (MARS-F) show strong screening of resonant field components

- Ideal magneto-hydrodynamics (MHD) suggests screening of resonant fields
- Strong **screening** response is recoved in resistive single fluid (MARS-F) calculations

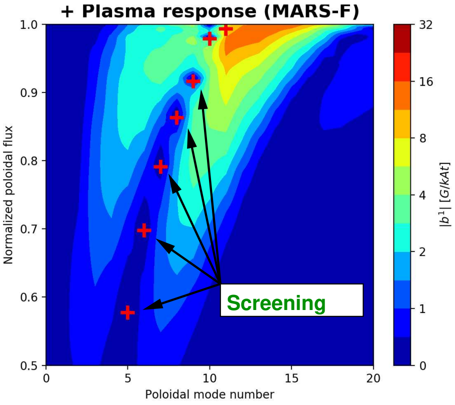

Resistive single fluid calculations (MARS-F) show strong screening of resonant field components

- Ideal magneto-hydrodynamics (MHD) suggests screening of resonant fields
- Strong **screening** response is recoved in resistive single fluid (MARS-F) calculations
- But plasma response includes field **amplification** near separatrix

  $\rightarrow$ important for divertor operation

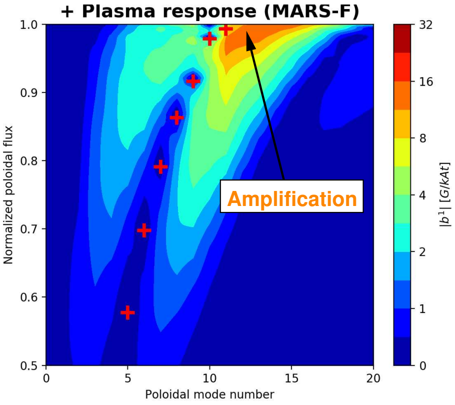

Plasma response affects size and radial connection of magnetic footprint

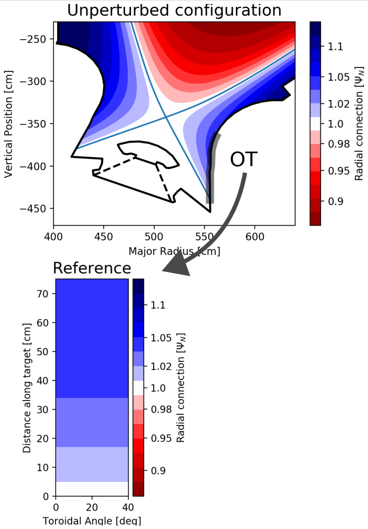

Plasma response affects size and radial connection of magnetic footprint

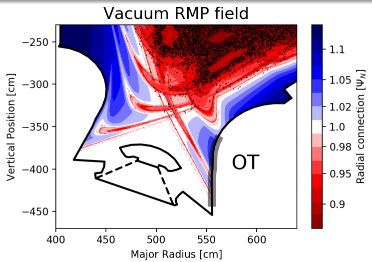

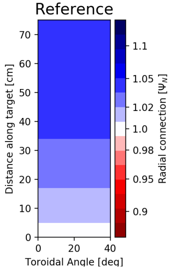

Plasma response affects size and radial connection of magnetic footprint

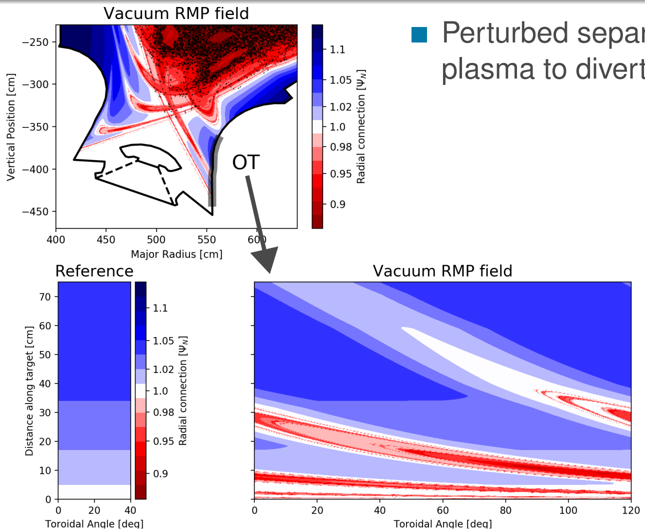

- Perturbed separatrix guides field lines from the bulk plasma to divertor targets

Plasma response affects size and radial connection of magnetic footprint

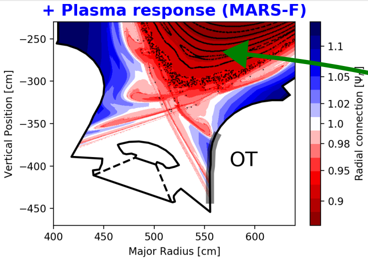

- Perturbed separatrix guides field lines from the bulk plasma to divertor targets
- **Screening**: reduced radial extent of perturbed SOL

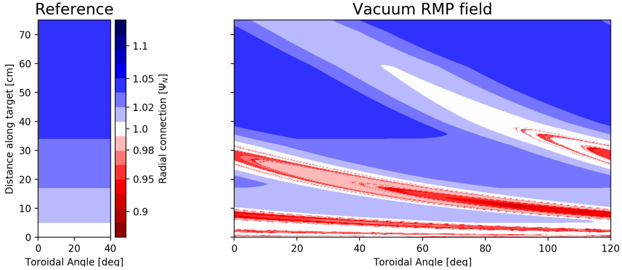

Plasma response affects size and radial connection of magnetic footprint

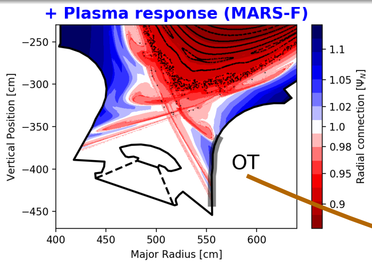

- Perturbed separatrix guides field lines from the bulk plasma to divertor targets
- **Screening**: reduced radial extent of perturbed SOL
- But large non-axisymmetric footprint from field **amplification** in competition with screening

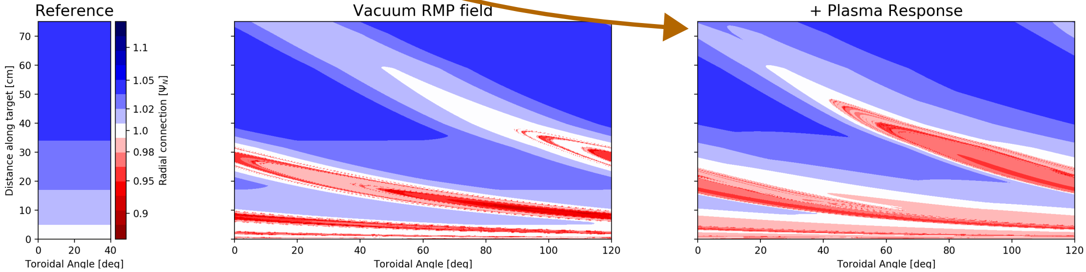

Outline

EMC3-EIRENE simulations show heat flux peaking correlated with radial connection of perturbed field lines

- Model parameters: $\Gamma_{gas} = 3 \cdot 10^{22}\,\mathrm{s}^{-1}$, $P_{SOL} = 30\,\mathrm{MW}$, $D_\perp = 0.3\,\mathrm{m}^2\,\mathrm{s}^{-1}$, $\chi_\perp = 1\,\mathrm{m}^2\,\mathrm{s}^{-1}$

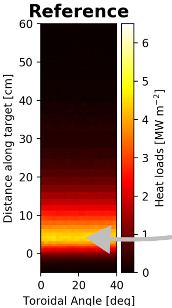

- Reference (unperturbed) configuration still attached

EMC3-EIRENE simulations show heat flux peaking correlated with radial connection of perturbed field lines

- Model parameters: $\Gamma_{\mathrm{gas}} = 3 \cdot 10^{22}\,\mathrm{s}^{-1}$, $P_{\mathrm{SOL}} = 30\,\mathrm{MW}$, $D_\perp = 0.3\,\mathrm{m}^2\,\mathrm{s}^{-1}$, $\chi_\perp = 1\,\mathrm{m}^2\,\mathrm{s}^{-1}$

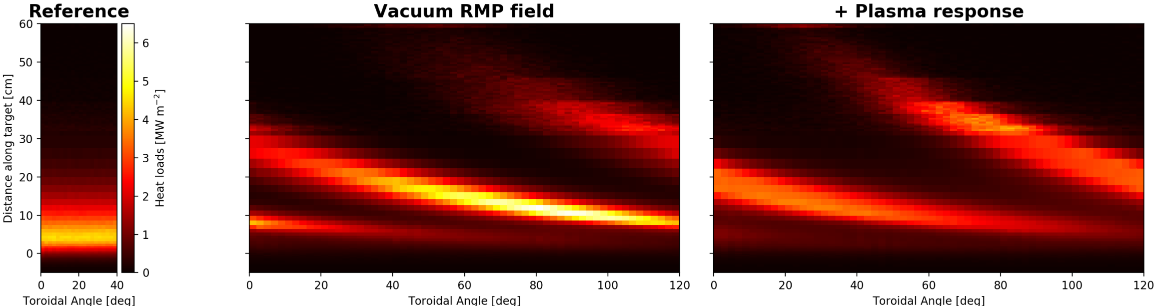

EMC3-EIRENE simulations show heat flux peaking correlated with radial connection of perturbed field lines

- Model parameters: $\Gamma_{gas} = 3 \cdot 10^{22}\,\mathrm{s}^{-1}$, $P_{SOL} = 30\,\mathrm{MW}$, $D_\perp = 0.3\,\mathrm{m}^2\,\mathrm{s}^{-1}$, $\chi_\perp = 1\,\mathrm{m}^2\,\mathrm{s}^{-1}$

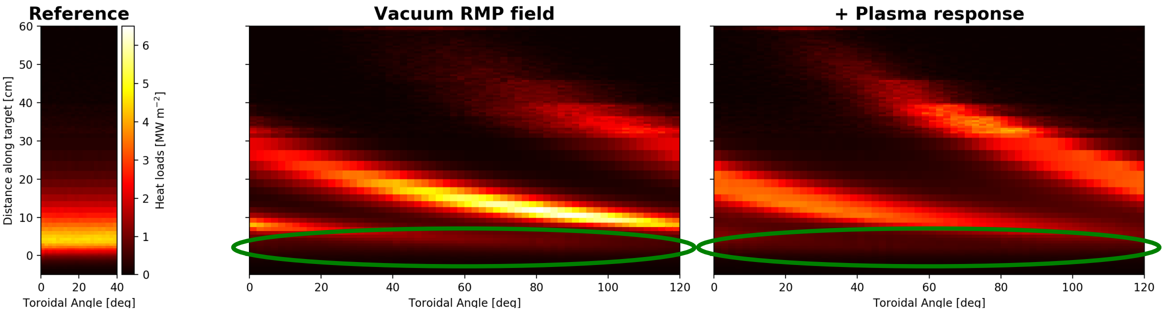

- RMPs: **earlier onset of detachment** in original strike zone (OSZ)

EMC3-EIRENE simulations show heat flux peaking correlated with radial connection of perturbed field lines

- Model parameters: $\Gamma_{\mathrm{gas}} = 3 \cdot 10^{22}\,\mathrm{s}^{-1}$, $P_{\mathrm{SOL}} = 30\,\mathrm{MW}$, $D_{\perp} = 0.3\,\mathrm{m}^2\,\mathrm{s}^{-1}$, $\chi_{\perp} = 1\,\mathrm{m}^2\,\mathrm{s}^{-1}$

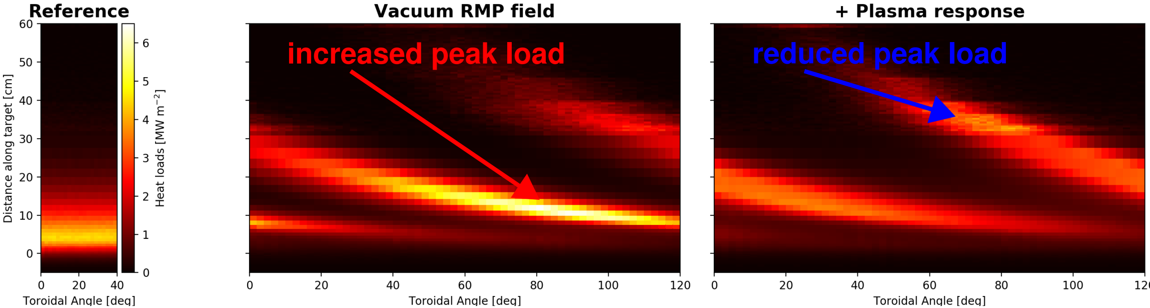

- RMPs: **earlier onset of detachment** in original strike zone (OSZ)
- Far SOL remains attached with heat flux peaking away from OSZ

EMC3-EIRENE simulations show heat flux peaking correlated with radial connection of perturbed field lines

- Model parameters: $\Gamma_{gas} = 3 \cdot 10^{22}\,\mathrm{s}^{-1}$, $P_{SOL} = 30\,\mathrm{MW}$, $D_{\perp} = 0.3\,\mathrm{m}^2\,\mathrm{s}^{-1}$, $\chi_{\perp} = 1\,\mathrm{m}^2\,\mathrm{s}^{-1}$

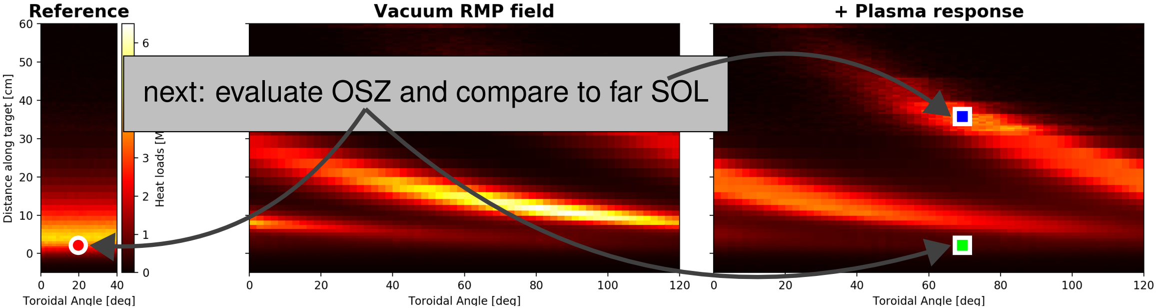

next: evaluate OSZ and compare to far SOL

- RMPs: **earlier onset of detachment** in original strike zone (OSZ)
- Far SOL remains attached with heat flux peaking away from OSZ

RMPs: significantly different exhaust characteristics at primary and secondary strike locations

- Divertor performance is evaluated with gas puff (density) scan
- Particle flux **roll-over** found in reference (unperturbed) configuration

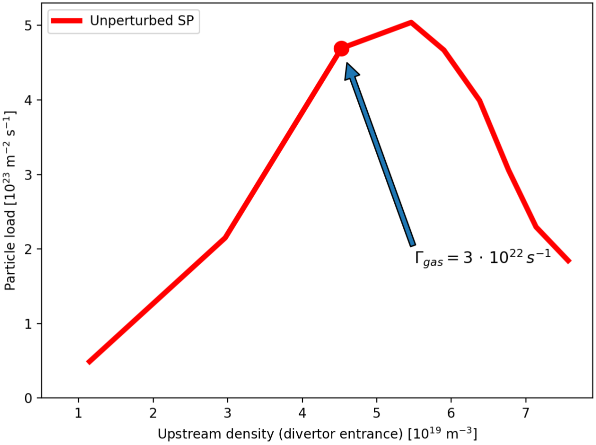

RMPs: significantly different exhaust characteristics at primary and secondary strike locations

- Divertor performance is evaluated with gas puff (density) scan
- Particle flux **roll-over** found in reference (unperturbed) configuration
- **Early detachment** of primary perturbed strike location

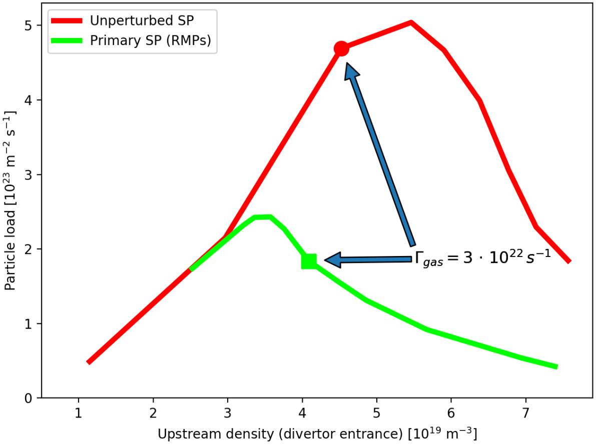

RMPs: significantly different exhaust characteristics at primary and secondary strike locations

- Divertor performance is evaluated with gas puff (density) scan
- Particle flux **roll-over** found in reference (unperturbed) configuration
- **Early detachment** of primary perturbed strike location
- Secondary perturbed strike location **remains attached**

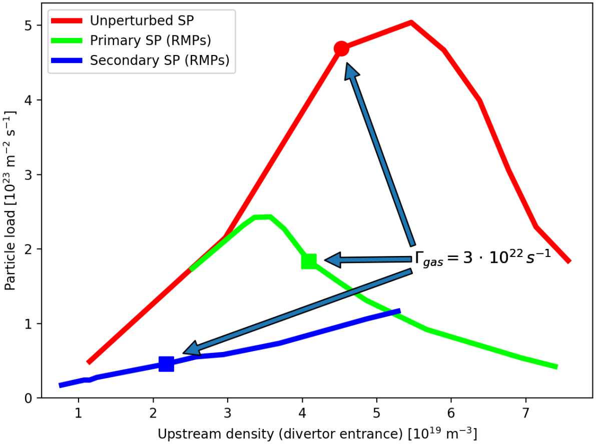

Leading role of T_t facilitates parametrization of characteristic curves for divertor operation

- Boundary condition sets link between particle and heat loads:

$$\Gamma_t = \frac{q_t}{\gamma T_t}, \qquad Q_t = \underbrace{q_t}_{\text{thermal load}} + \underbrace{\varepsilon \Gamma_t}_{\text{from surface recombination}}$$

Leading role of T_t facilitates parametrization of characteristic curves for divertor operation

- Boundary condition sets link between particle and heat loads:

$$\Gamma_t = \frac{q_t}{\gamma\, T_t}, \qquad Q_t = q_t + \varepsilon\, \Gamma_t$$

- Power losses in the divertor provide link to heat flux from bulk plasma:

$$q_t = (1 - f_{\mathrm{cool}}) \cdot \underbrace{q_{||} \cdot B_t / B_u \cdot \sin\vartheta}_{=\widehat{q}}$$

Leading role of T_t facilitates parametrization of characteristic curves for divertor operation

- Boundary condition sets link between particle and heat loads:

$$\Gamma_t = \frac{q_t}{\gamma\, T_t}, \qquad Q_t = q_t + \varepsilon\, \Gamma_t$$

- Power losses in the divertor provide link to heat flux from bulk plasma:

$$q_t = (1 - f_{\mathrm{cool}}) \cdot \underbrace{q_{\|} \cdot B_t / B_u \cdot \sin\vartheta}_{=\,\widehat{q}}$$

- Parametrization of f_{cool}:

$$1 - f_{\mathrm{cool}}(T_t) = \boxed{A} \left(1 - e^{-T_t/\boxed{T^*}}\right)^{\boxed{\alpha}}$$

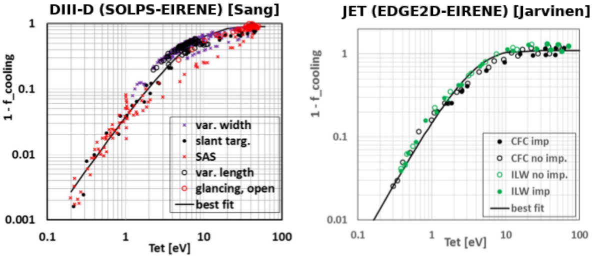

$A = 0.9 - 1.1, \qquad T^* = 2.4 - 6, \qquad \alpha = 1.6 - 1.9$

P.C. Stangeby PPCF **60** (2018) 044022

Leading role of T_t facilitates parametrization of characteristic curves for divertor operation

- Boundary condition sets link between particle and heat loads:

$$\Gamma_t = \frac{q_t}{\gamma\, T_t}, \qquad Q_t = q_t + \varepsilon\, \Gamma_t$$

- Power losses in the divertor provide link to heat flux from bulk plasma:

$$q_t = (1 - f_{\mathrm{cool}}) \cdot \underbrace{q_{\|} \cdot B_t / B_u \cdot \sin\vartheta}_{= \hat{q}}$$

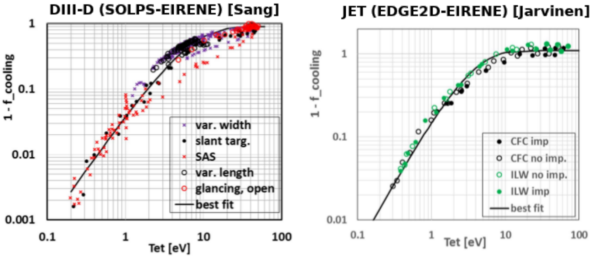

$$A = 0.9 - 1.1, \qquad T^* = 2.4 - 6, \qquad \alpha = 1.6 - 1.9$$

P.C. Stangeby PPCF **60** (2018) 044022

- Parametrization of f_{cool}:

$$1 - f_{\mathrm{cool}}(T_t) = A \left(1 - e^{-T_t/T^*}\right)^{\alpha}$$

high T_t limit

when onset happens

how fast losses take over after that

Leading role of T_t facilitates parametrization of characteristic curves for divertor operation

- Boundary condition sets link between particle and heat loads:

$$\Gamma_t = \frac{q_t}{\gamma\, T_t}, \qquad Q_t = q_t + \varepsilon\, \Gamma_t$$

- Power losses in the divertor provide link to heat flux from bulk plasma:

$$q_t = (1 - f_{\mathrm{cool}}) \cdot \underbrace{q_{||} \cdot B_t / B_u \cdot \sin\vartheta}_{=\hat{q}}$$

- Parametrization of f_{cool}:

$$1 - f_{\mathrm{cool}}(T_t) = A \left(1 - e^{-T_t / T^*}\right)^{\alpha}$$

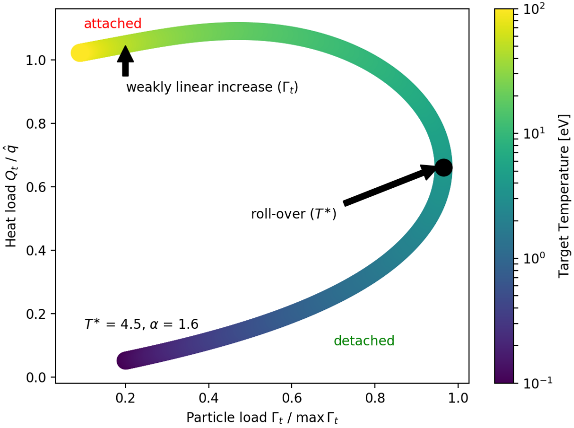

Qualitative explanation by splitting of upstream heat flux and different radial field line connections

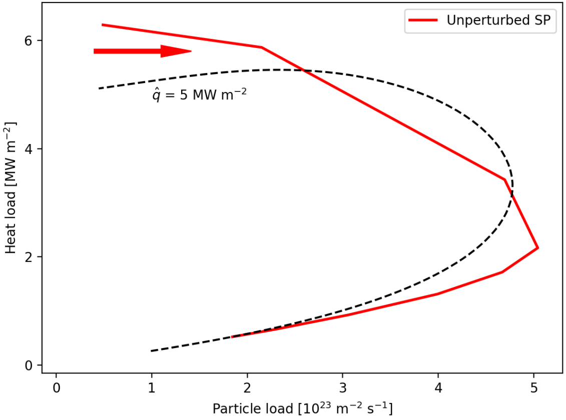

- Toy model captures roll-over of unperturbed SP

Qualitative explanation by splitting of upstream heat flux and different radial field line connections

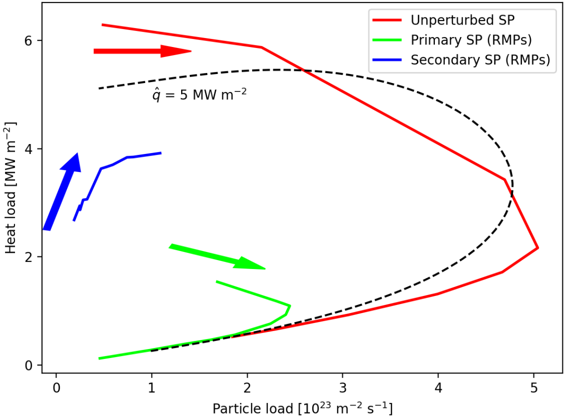

- Toy model captures roll-over of unperturbed SP

Qualitative explanation by splitting of upstream heat flux and different radial field line connections

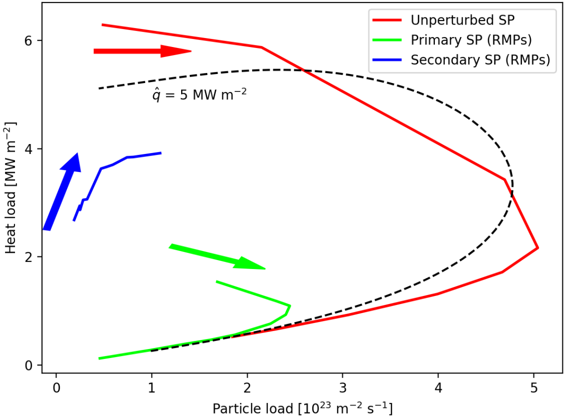

- Toy model captures roll-over of unperturbed SP

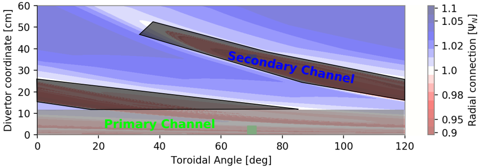

Qualitative explanation by splitting of upstream heat flux and different radial field line connections

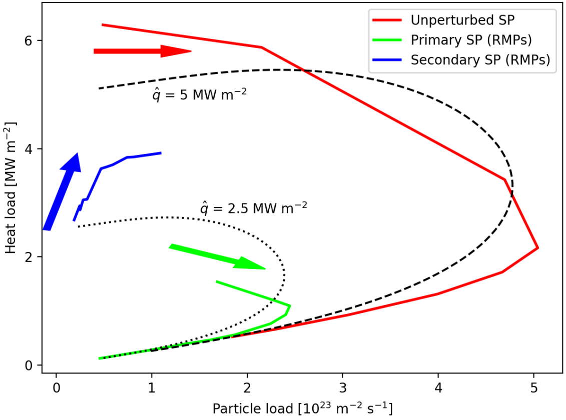

- Toy model captures roll-over of unperturbed SP

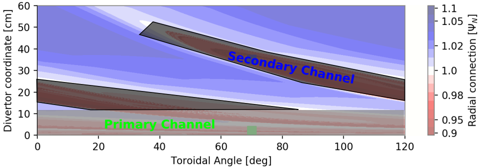

- Splitting of perturbed heat flux consistent with reduction of peak particle load by factor 2

Qualitative explanation by splitting of upstream heat flux and different radial field line connections

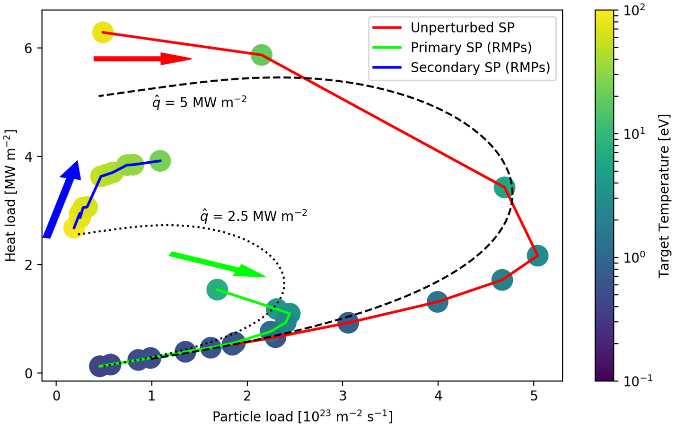

- Toy model captures roll-over of unperturbed SP

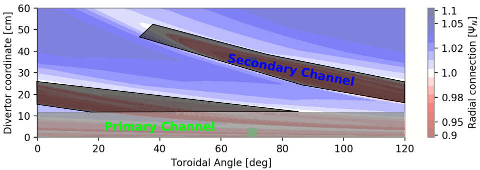

- Splitting of perturbed heat flux consistent with reduction of peak particle load by factor 2

- Primary SP is on low T_t branch ahead of seconday SP on same (type of) curve

Qualitative explanation by splitting of upstream heat flux and different radial field line connections

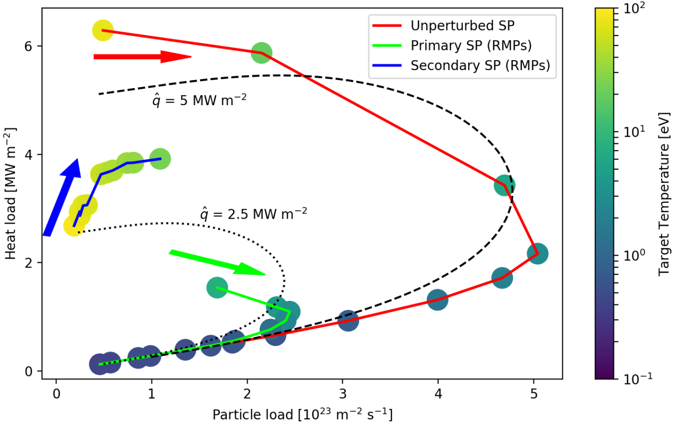

- Toy model captures roll-over of unperturbed SP

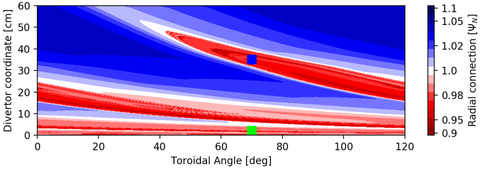

- Splitting of perturbed heat flux consistent with reduction of peak particle load by factor 2

- Primary SP is on low T_t branch ahead of seconday SP on same (type of) curve

Qualitative explanation by splitting of upstream heat flux and different radial field line connections

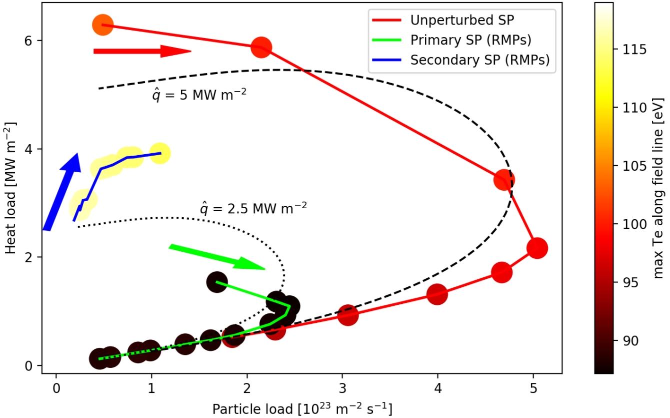

- Toy model captures roll-over of unperturbed SP

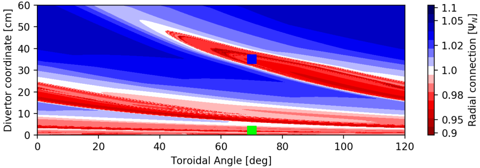

- Splitting of perturbed heat flux consistent with reduction of peak particle load by factor 2

- Primary SP is on low T_t branch ahead of seconday SP on same (type of) curve
- Higher T_t consistent with **deeper radial connection** from secondary SP to higher T_u

Outline

Footprint size is sensitive to rotation profile in MARS-F

- **Amplification** competes with **screening**, and depends on assumed rotation profile

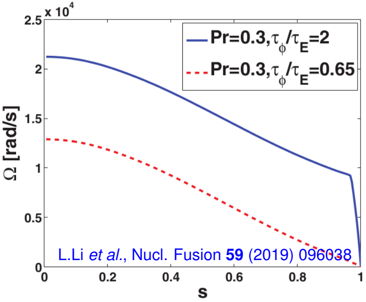

Footprint size is sensitive to rotation profile in MARS-F

- **Amplification** competes with **screening**, and depends on assumed rotation profile

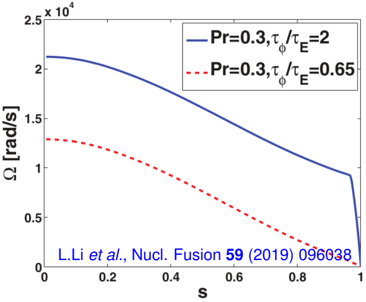

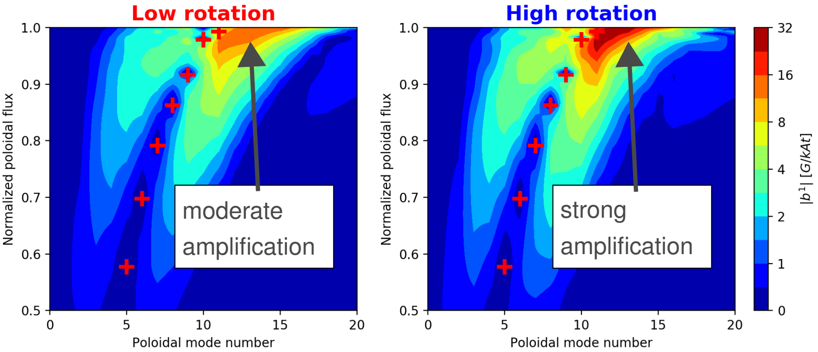

Footprint size is sensitive to rotation profile in MARS-F

- **Amplification** competes with **screening**, and depends on assumed rotation profile
- Significant extension of footprint possible from strong amplification near separatrix

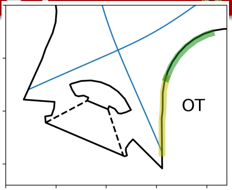

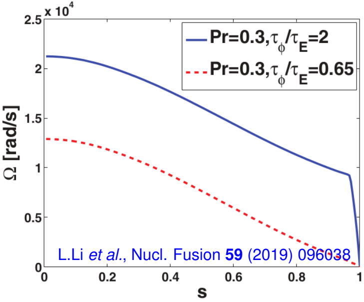

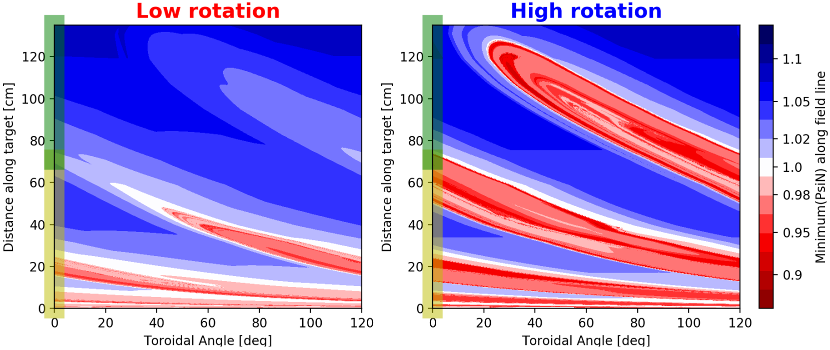

Footprint size is sensitive to rotation profile in MARS-F

- **Amplification** competes with **screening**, and depends on assumed rotation profile
- Significant extension of footprint possible from strong amplification near separatrix

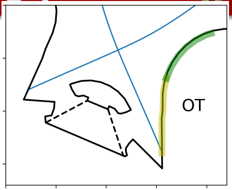

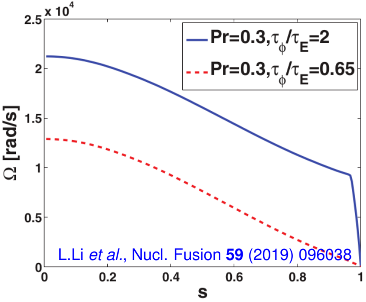

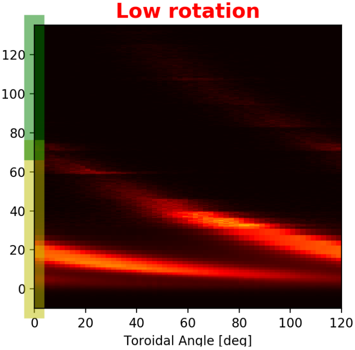

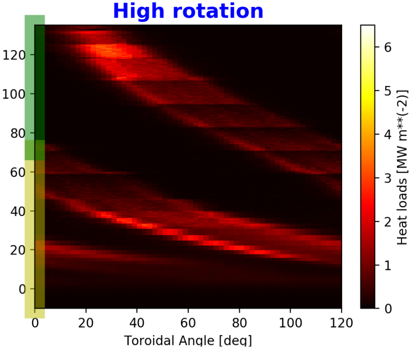

- Heat loads may occur far outside of **dedicated high heat flux region**

Footprint size is sensitive to rotation profile in MARS-F

- **Amplification** competes with **screening**, and depends on assumed rotation profile
- Significant extension of footprint possible from strong amplification near separatrix

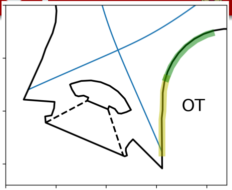

Optimal coil phasing for ELM control may not be optimal for divertor operation at full power → rotate RMPs

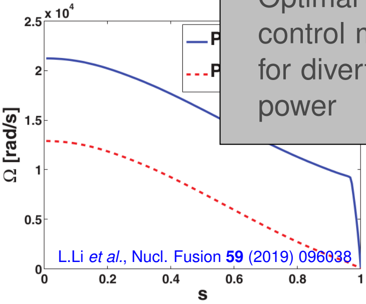

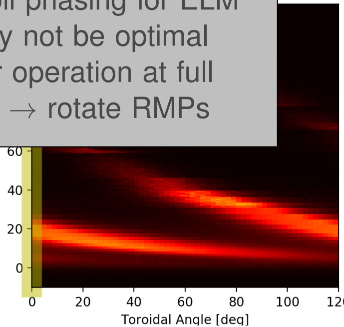

High rotation

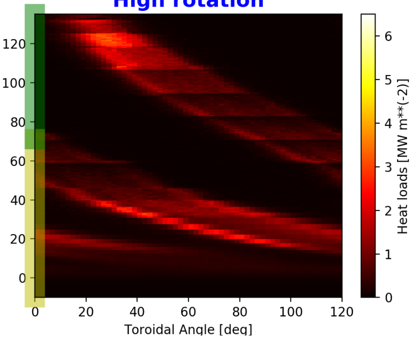

- Heat loads may occur far outside of **dedicated high heat flux region**

Optimal ELM control phasings imply large footprint size

- ELM control optimized based on displacement near X-point
- Footprint size s: max. distance from original strike point with connection to $\Psi_N < 1$

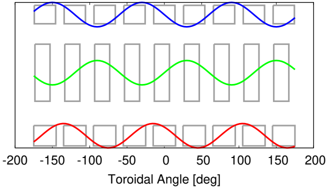

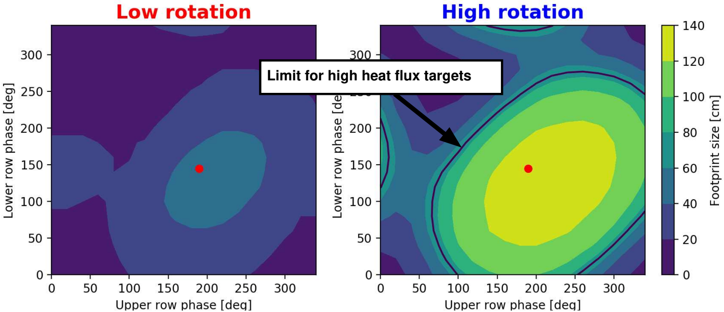

- Reduced divertor closure at $s \gtrsim 70\,\mathrm{cm}$ (soft limit), and extension beyond dedicated high heat flux region (hard limit at full power?) $\rightarrow$ **reliable prediction of plasma response required!**

Conclusions

1. An earlier transition to detachment is found at the OSZ with RMPs while the far SOL non-axisymmetric SP remains attached

   $\rightarrow$ **high** T_t at secondary SP is problematic for extrinsic impurities required for dissipation at full power

2. Non-axisymmetric particle and heat loads during RMP application are sensitive to the **plasma response** (in particular the toroidal rotation used in MARS-F)

   $\rightarrow$ Optimal coil phasing for ELM control not optimal for divertor operation? (rotation of RMPs possible but should be avoided)

   $\rightarrow$ **Reliable predictions for plasma response models required!**

APPENDIX

Plasma response determines radial extent of perturbed SOL

- Screening response: smaller, non-overlapping island chains
  $\rightarrow$ reduced radial extent of perturbed SOL

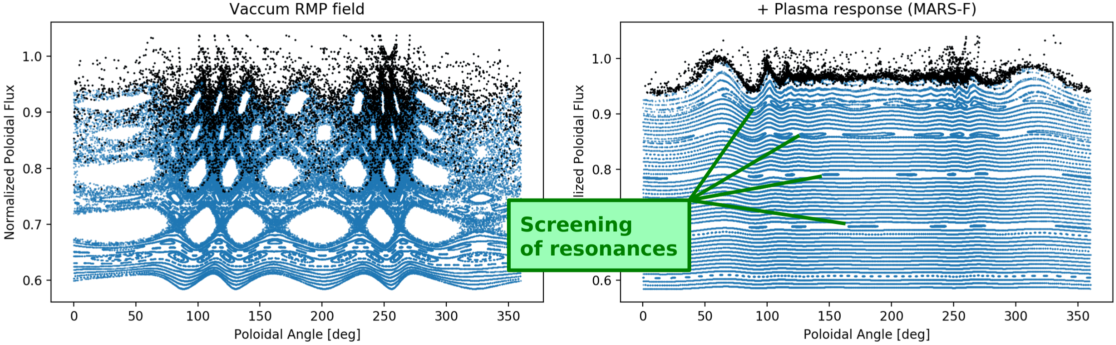

Plasma response determines radial extent of perturbed SOL

- Screening response: smaller, non-overlapping island chains
  $\rightarrow$ reduced radial extent of perturbed SOL
- Perturbed SOL: field lines connect to divertor targets

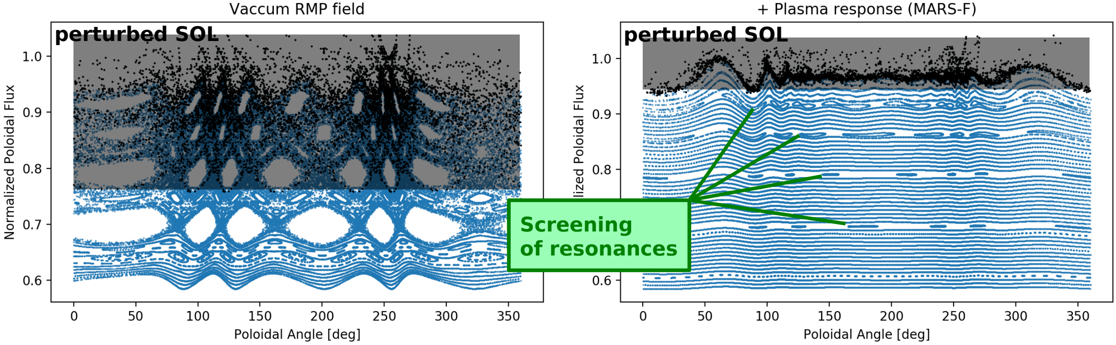

Plasma response determines radial extent of perturbed SOL

- Screening response: smaller, non-overlapping island chains
  $\rightarrow$ reduced radial extent of perturbed SOL
- Perturbed SOL: field lines connect to divertor targets
  $\rightarrow$ higher edge temperature can be sustained with RMP screening

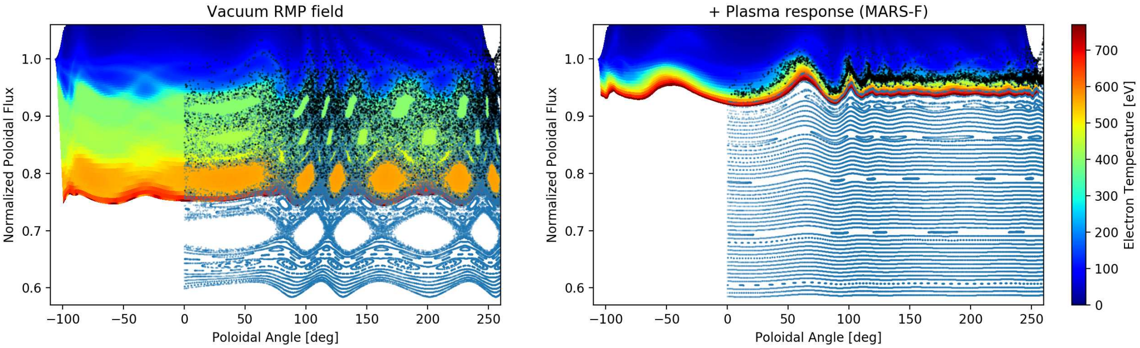

Heat loads may occur far from original strike zone depending on plasma response

- Model parameters: $\Gamma_{gas} = 3 \cdot 10^{22}\,\mathrm{s}^{-1}$, $P_{edge} = 30\,\mathrm{MW}$, $D_\perp = 0.3\,\mathrm{m}^2\,\mathrm{s}^{-1}$, $\chi_\perp = 1\,\mathrm{m}^2\,\mathrm{s}^{-1}$

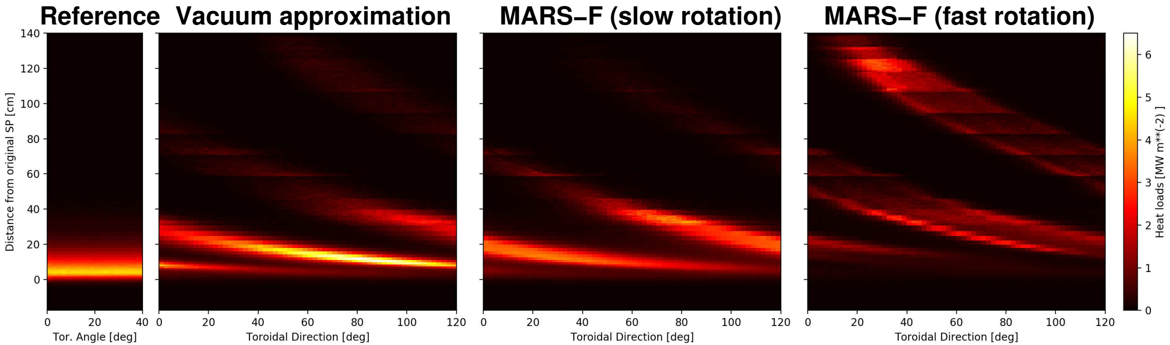

- Optimal coil phasing for ELM control may not be optimal for divertor operation

Screening competes with field amplification near separatrix

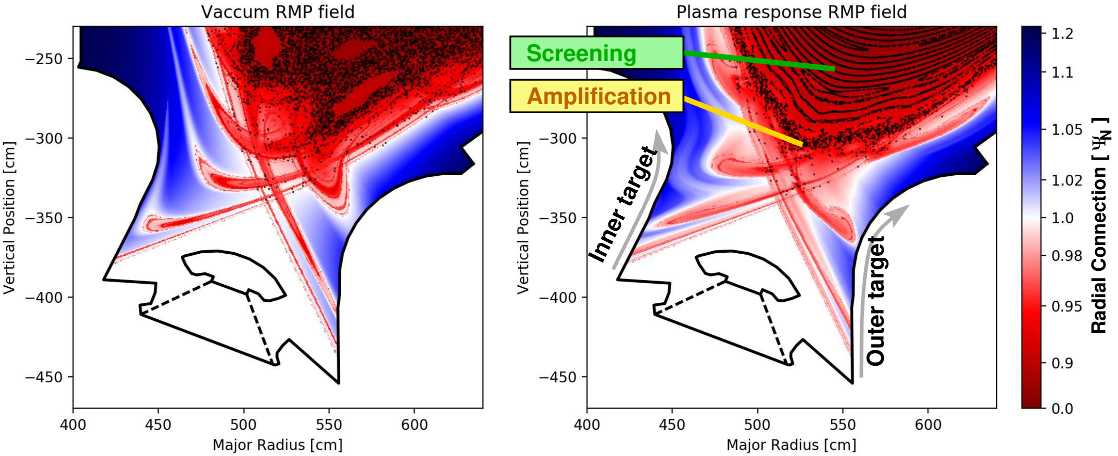

- MARS-F plasma response includes both **screening** of resonances within the bulk plasma and **amplification** near the separatrix

Absence of power and momentum losses confirm: secondary SP (RMPs) remains attached

- Evaluate power and momentum losses with respect to divertor entrance:

$$1 - f_{\mathrm{cool}} = q_t / q_u^{(\mathrm{tot.})} \qquad 1 - f_{\mathrm{mom}} = p_t^{(\mathrm{tot.})} / p_u^{(\mathrm{tot.})}$$

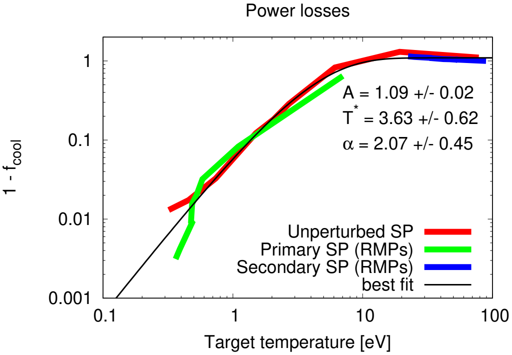

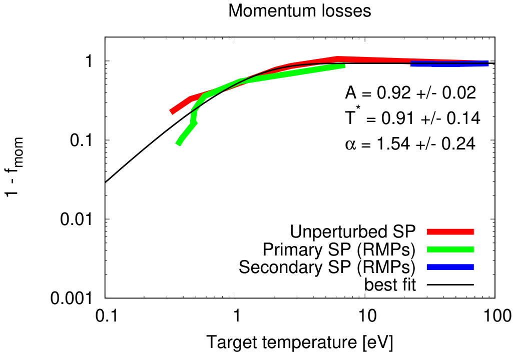

What are the implications of 2ndary SP for divertor operation?

- Initially even weaker T_t scaling than traditional attached conditions ($T_t \sim \Gamma_t^{-1}$) because of **increasing** $\hat{q}$

  $\rightarrow$ increasing q_t observed at EAST (J. Li, Nature Physics **9** 817 (2013))

- High T_t increases sputtering on tungsten plates

- Field lines connect deeper into the plasma

  $\rightarrow$ even higher T_u at full power

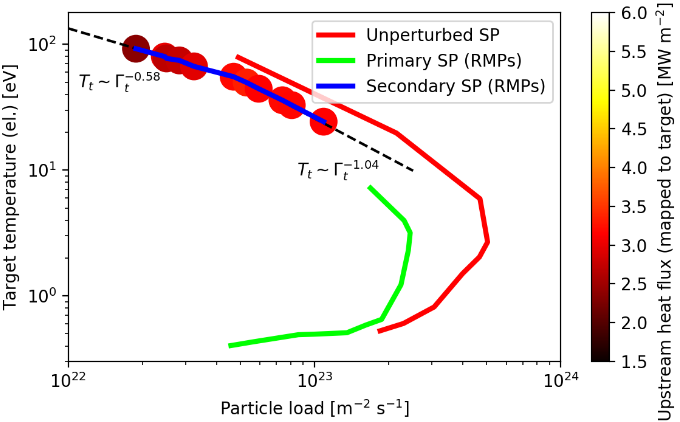

- From divertor entrance (X-point) to targets: shorter connection length

  $\rightarrow$ less dissipation possible (even if T_t can be brought down)

Linearization of S_{ee} provides stabilization at low divertor temperatures

- First order Taylor expansion allows more accurate treatment of T_e dependence:

$$S_{ee}^{(j)} \approx S_{ee}\left(T_e^{(j-1)}\right) + \left(T_e^{(j)} - T_e^{(j-1)}\right) \left.\frac{dS_{ee}}{dT_e}\right|_{T_e^{(j-1)}}$$

Linearization of S_{ee} provides stabilization at low divertor temperatures

- First order Taylor expansion allows more accurate treatment of T_e dependence:

$$S_{ee}^{(j)} \approx S_{ee}\left(T_e^{(j-1)}\right) + \left(T_e^{(j)} - T_e^{(j-1)}\right) \left.\frac{dS_{ee}}{dT_e}\right|_{T_e^{(j-1)}}$$

- Source decomposition (linearization) can be stabilizing if $S_{ee1} \leq 0$:

$$S_{ee} \approx S_{ee0} + T_e \cdot S_{ee1}$$

explicit method

implicit method

Linearization of S_{ee} provides stabilization at low divertor temperatures

- First order Taylor expansion allows more accurate treatment of T_e dependence:

$$S_{ee}^{(j)} \approx S_{ee}\left(T_e^{(j-1)}\right) + \left(T_e^{(j)} - T_e^{(j-1)}\right) \left.\frac{dS_{ee}}{dT_e}\right|_{T_e^{(j-1)}}$$

- Source decomposition (linearization) can be stabilizing if $S_{ee1} \leq 0$:

$$S_{ee} \approx S_{ee0} + T_e \cdot S_{ee1}$$

explicit method

implicit method

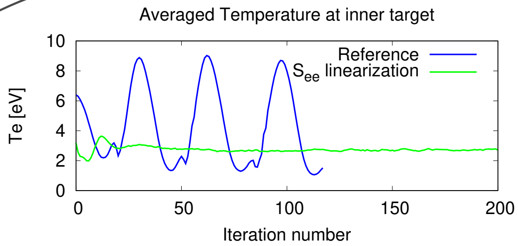

EMC3: A 3D fluid model for the (steady state) edge plasma

Particle balance (n: plasma density)

Y. Feng et al. *PPCF* **59** (2017) 034006

$$\nabla \cdot \left[n u_{||} \mathbf{e}_{||} - D_\perp \mathbf{e}_\perp \mathbf{e}_\perp \cdot \nabla n \right] = S_p$$

$D_\perp$: anomalous cross-field diffusion, S_p: ionization of neutral particles

EMC3: A 3D fluid model for the (steady state) edge plasma

Particle balance (n: plasma density)

Y. Feng et al. *PPCF* **59** (2017) 034006

$$\nabla \cdot \left[n u_{||} \mathbf{e}_{||} - D_\perp \mathbf{e}_\perp \mathbf{e}_\perp \cdot \nabla n \right] = S_p$$

Momentum balance ($u_{||}$: fluid velocity parallel to magnetic field lines)

$$\nabla \cdot \left[m_i n u_{||}^2 \mathbf{e}_{||} - \eta_{||} \mathbf{e}_{||} \mathbf{e}_{||} \cdot \nabla u_{||} - D_\perp \mathbf{e}_\perp \mathbf{e}_\perp \cdot \nabla \left(m_i n u_{||} \right) \right] = -\mathbf{e}_{||} \cdot \nabla n \left(T_e + T_i \right) + S_m$$

$\eta_\perp = m_i n D_\perp$: anomalous cross-field viscosity, S_m: interaction (CX) with neutral particles

EMC3: A 3D fluid model for the (steady state) edge plasma

Particle balance (n: plasma density)

Y. Feng et al. *PPCF* **59** (2017) 034006

$$\nabla \cdot \left[n u_{\|} \mathbf{e}_{\|} - D_{\perp} \mathbf{e}_{\perp} \mathbf{e}_{\perp} \cdot \nabla n \right] = S_p$$

Momentum balance ($u_{\|}$: fluid velocity parallel to magnetic field lines)

$$\nabla \cdot \left[m_i n u_{\|}^2 \mathbf{e}_{\|} - \eta_{\|} \mathbf{e}_{\|} \mathbf{e}_{\|} \cdot \nabla u_{\|} - D_{\perp} \mathbf{e}_{\perp} \mathbf{e}_{\perp} \cdot \nabla \left(m_i n u_{\|} \right) \right] = -\mathbf{e}_{\|} \cdot \nabla n \left(T_e + T_i \right) + S_m$$

Energy balance (T_e, T_i: electron and ion temperature)

$$\nabla \cdot \left[\frac{5}{2} T_e \left(n u_{\|} \mathbf{e}_{\|} - D_{\perp} \mathbf{e}_{\perp} \mathbf{e}_{\perp} \cdot \nabla n \right) - \left(\kappa_e \mathbf{e}_{\|} \mathbf{e}_{\|} + \chi_e n \mathbf{e}_{\perp} \mathbf{e}_{\perp} \right) \cdot \nabla T_e \right] = +K \left(T_i - T_e \right) + S_{ee} + S_{e,imp}$$

$$\nabla \cdot \left[\frac{5}{2} T_i \left(n u_{\|} \mathbf{e}_{\|} - D_{\perp} \mathbf{e}_{\perp} \mathbf{e}_{\perp} \cdot \nabla n \right) - \left(\kappa_i \mathbf{e}_{\|} \mathbf{e}_{\|} + \chi_i n \mathbf{e}_{\perp} \mathbf{e}_{\perp} \right) \cdot \nabla T_i \right] = -K \left(T_i - T_e \right) + S_{ei}$$

χ_e, χ_i: anomalous cross-field transport

$S_{e\ldots}$: interaction with neutral particles and impurities

EMC3: A 3D fluid model for the (steady state) edge plasma

Particle balance (n: plasma density)

Y. Feng et al. *PPCF* **59** (2017) 034006

$$\nabla \cdot \left[n u_{\|} \mathbf{e}_{\|} - D_{\perp} \mathbf{e}_{\perp} \mathbf{e}_{\perp} \cdot \nabla n \right] = S_p$$

Momentum balance ($u_{\|}$: fluid velocity parallel to magnetic field lines)

$$\nabla \cdot \left[m_i n u_{\|}^2 \mathbf{e}_{\|} - \eta_{\|} \mathbf{e}_{\|} \mathbf{e}_{\|} \cdot \nabla u_{\|} - D_{\perp} \mathbf{e}_{\perp} \mathbf{e}_{\perp} \cdot \nabla \left(m_i n u_{\|} \right) \right] = -\mathbf{e}_{\|} \cdot \nabla n \left(T_e + T_i \right) + S_m$$

Energy balance (T_e, T_i: electron and ion temperature)

$$\nabla \cdot \left[\frac{5}{2} T_e \left(n u_{\|} \mathbf{e}_{\|} - D_{\perp} \mathbf{e}_{\perp} \mathbf{e}_{\perp} \cdot \nabla n \right) - \left(\kappa_e \mathbf{e}_{\|} \mathbf{e}_{\|} + \chi_e n \mathbf{e}_{\perp} \mathbf{e}_{\perp} \right) \cdot \nabla T_e \right] = +K \left(T_i - T_e \right) + S_{ee} + S_{e,imp}$$

$$\nabla \cdot \left[\frac{5}{2} T_i \left(n u_{\|} \mathbf{e}_{\|} - D_{\perp} \mathbf{e}_{\perp} \mathbf{e}_{\perp} \cdot \nabla n \right) - \left(\kappa_i \mathbf{e}_{\|} \mathbf{e}_{\|} + \chi_i n \mathbf{e}_{\perp} \mathbf{e}_{\perp} \right) \cdot \nabla T_i \right] = -K \left(T_i - T_e \right) + S_{ei}$$

χ_e, χ_i: anomalous cross-field transport

$S_{e\ldots}$: interaction with neutral particles and impurities

Energy losses are very sensitive at low temperature

- EIRENE: kinetic transport of neutral particles

  $\rightarrow n_H, n_{H_2}, n_{H_2^+}$

convolution of atomic and molecular processes

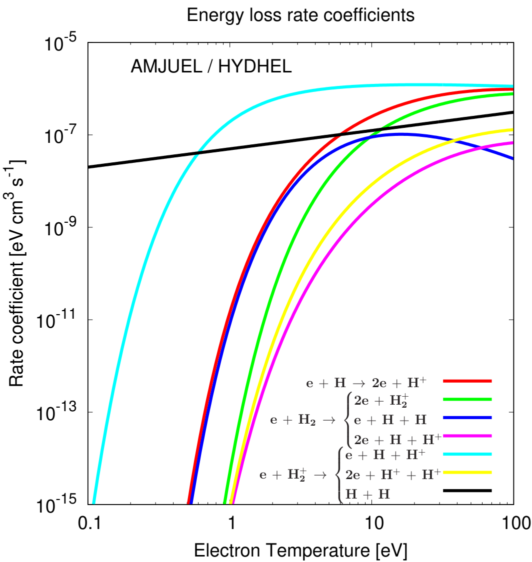

Energy losses are very sensitive at low temperature

- EIRENE: kinetic transport of neutral particles

$$\rightarrow n_H,\ n_{H_2},\ n_{H_2^+}$$

convolution of atomic and molecular processes

- Energy losses from electron impact processes:

$$S_{ee} = -\sum_X n_e \cdot n_{\ldots} \cdot R_X(T_e, n_e)$$

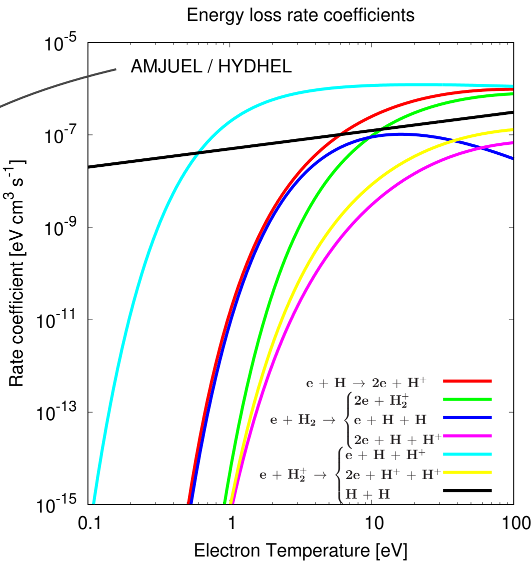

Energy losses are very sensitive at low temperature

- EIRENE: kinetic transport of neutral particles

  $$\rightarrow n_H,\ n_{H_2},\ n_{H_2^+}$$

  convolution of atomic and molecular processes

- Energy losses from electron impact processes:

  $$S_{ee} = -\sum_X n_e \cdot n_{\ldots} \cdot \boxed{R_X(T_e, n_e)}$$

- Iterative approximation of energy balance:

  $$S_{ee}^{(j)} \approx S_{ee}\left(T_e^{(j-1)}\right)$$

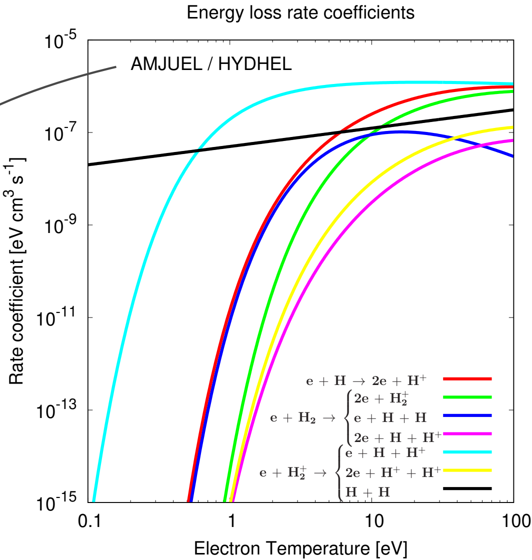

Linearization of S_{ee} provides stabilization at detachment relevant low divertor temperatures

attached conditions:

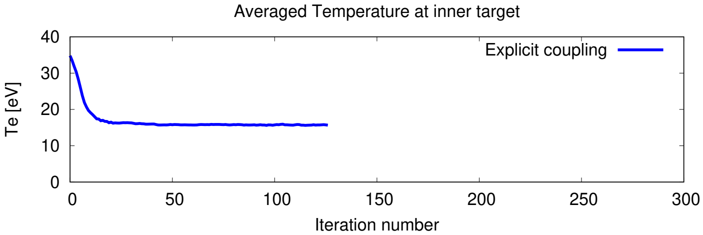

$$S_{ee}^{(j)} \approx \boxed{S_{ee}\left(T_e^{(j-1)}\right)}$$

Linearization of S_{ee} provides stabilization at detachment relevant low divertor temperatures

- Temperature dependence of S_{ee} is not treated accurately enough at low T_e relevant for detachment

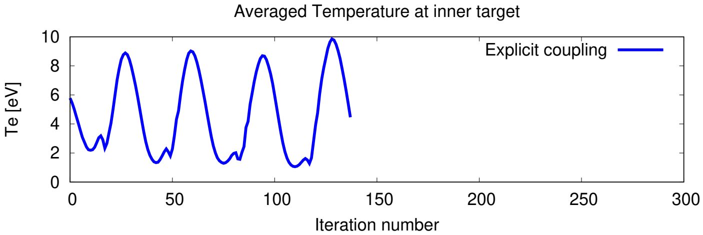

$$S_{ee}^{(j)} \approx \boxed{S_{ee}\left(T_e^{(j-1)}\right)}$$

Linearization of S_{ee} provides stabilization at detachment relevant low divertor temperatures

- Temperature dependence of S_{ee} is not treated accurately enough at low T_e relevant for detachment

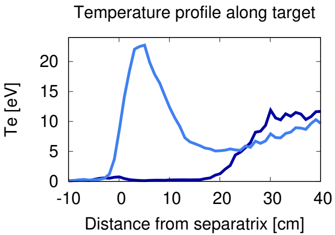

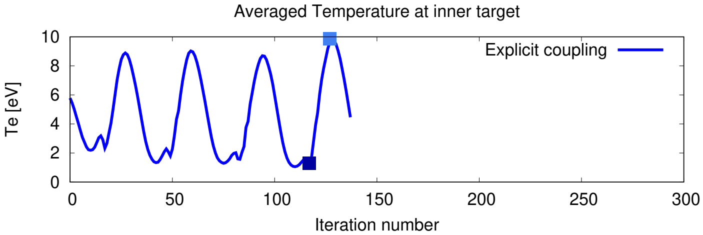

$$S_{ee}^{(j)} \approx \boxed{S_{ee}\left(T_e^{(j-1)}\right)}$$

Linearization of S_{ee} provides stabilization at detachment relevant low divertor temperatures

- Temperature dependence of S_{ee} is not treated accurately enough at low T_e relevant for detachment

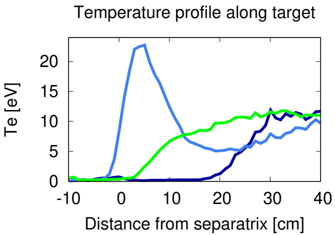

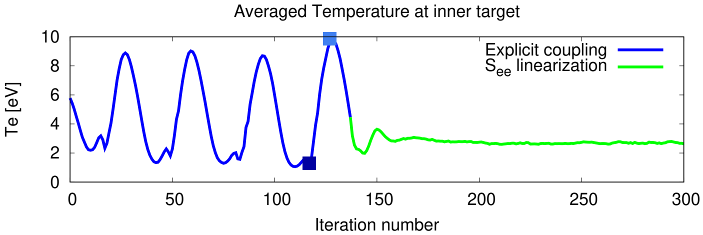

- More accurate treatment of T_e dependence based on first order Taylor expansion:

$$S_{ee}^{(j)} \approx \boxed{S_{ee}\left(T_e^{(j-1)}\right)} + \left(T_e^{(j)} - T_e^{(j-1)}\right) \boxed{\left.\frac{dS_{ee}}{dT_e}\right|_{T_e^{(j-1)}}}$$

Extended operation range of EMC3-EIRENE is verified by comparison to SOLPS-ITER

- H-plasma (PFPO, no seeded impurities), model parameters:
  $D_\perp = 0.3\,\mathrm{m}^2\,\mathrm{s}^{-1}$, $\chi_\perp = 1\,\mathrm{m}^2\,\mathrm{s}^{-1}$
- Self-consistent particle balance $\Gamma_{\mathrm{pump}} = \Gamma_{\mathrm{gas}} + \Gamma_{\mathrm{core}}$ including recirculation below the dome

  $\rightarrow$ Semi-transparent dome support (50 %)
  Pumping (0.72 %)
- Include N-N collisions (BGK), molecular assisted recombination (MAR)
- Fueling scan (Γ_{gas}) $\rightarrow$ evaluate neutral pressure & divertor loads

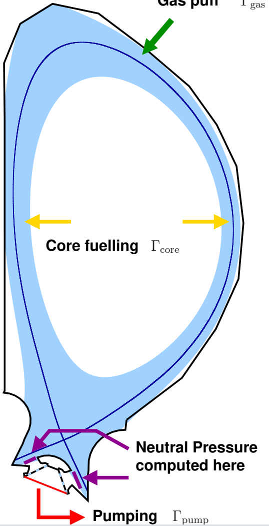

Extended operation range of EMC3-EIRENE is verified by comparison to SOLPS-ITER

- Continuous reduction of peak heat flux during gas puff scan

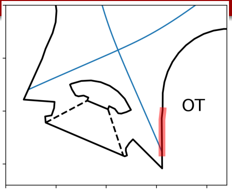

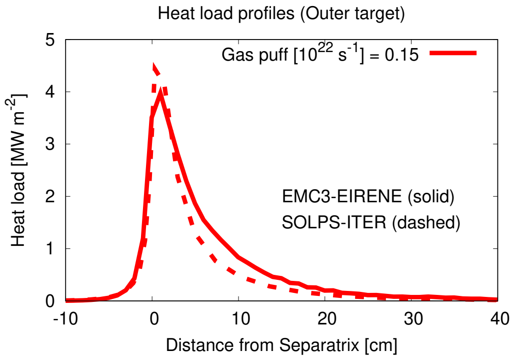

Extended operation range of EMC3-EIRENE is verified by comparison to SOLPS-ITER

- Continuous reduction of peak heat flux during gas puff scan

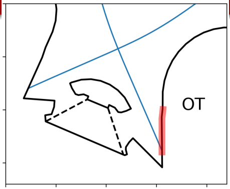

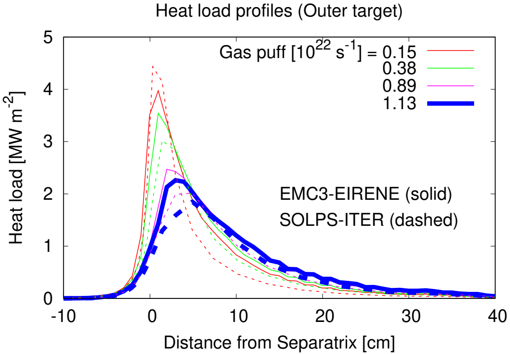

Extended operation range of EMC3-EIRENE is verified by comparison to SOLPS-ITER

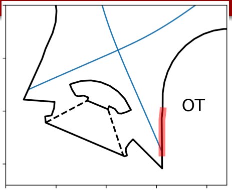

- Continuous reduction of peak heat flux during gas puff scan

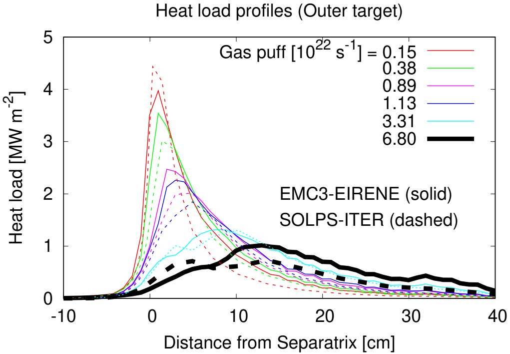

Extended operation range of EMC3-EIRENE is verified by comparison to SOLPS-ITER

- Continuous reduction of peak heat flux during gas puff scan
- A clear **roll-over** of peak particle flux is found by both codes in good agreement